

## ARTICLE

## OPEN



## Motility mediates satellite formation in confined biofilms

Mireia Cordero <sup>1</sup>, Namiko Mitarai <sup>1</sup>✉ and Liselotte Jauffred <sup>1</sup>✉

© The Author(s) 2023

Bacteria have spectacular survival capabilities and can spread in many, vastly different environments. For instance, when pathogenic bacteria infect a host, they expand by proliferation and squeezing through narrow pores and elastic matrices. However, the exact role of surface structures—important for biofilm formation and motility—and matrix density in colony expansion and morphogenesis is still largely unknown. Using confocal laser-scanning microscopy, we show how *satellite* colonies emerge around *Escherichia coli* colonies embedded in semi-dense hydrogel in controlled in vitro assays. Using knock-out mutants, we tested how extra-cellular structures, (e.g., exo-polysaccharides, flagella, and fimbria) control this morphology. Moreover, we identify the extra-cellular matrix' density, where this morphology is possible. When paralleled with mathematical modelling, our results suggest that satellite formation allows bacterial communities to spread faster. We anticipate that this strategy is important to speed up expansion in various environments, while retaining the close interactions and protection provided by the community.

*The ISME Journal* (2023) 17:1819–1827; <https://doi.org/10.1038/s41396-023-01494-x>

## INTRODUCTION

While many bacterial species can grow as free-swimming cells in planktonic mode, they will often adhere to a substrate or small enclosure to form dense communities like biofilms [1]. The biofilm community offers protection from local threats. For instance, against the shear flow by attaching to a solid substrate or by protecting the inner cells from the immune system, toxins, or bacteriophages [2, 3]. Also, the local, high cell density helps bacteria share necessary chemicals within the community [4]. The importance of biofilm formation is also reflected in the fact that bacteria have many genes contributing to cell-adhesive structures, such as exo-polysaccharides (EPS), fimbriae, and flagella [5]. These biofilms often grow—as the name indicates—as quasi-two-dimensional (2D) colonies on substrates, but also as three-dimensional (3D) communities in habitats, such as gels, tissues (e.g., the human gut), and soils. Despite this high prevalence, we still lack a full understanding of how dynamic morphologies of 3D biofilms are controlled.

When a bacterial community grows as a dense colony, the surface expands outwards as cells are proliferating, with a doubling time close to what we know from well-mixed liquid cultures. Behind the fast-growing pioneering cells on the front, is a quiescent region, where proliferation is slowed down significantly, due to space constraints [6] and metabolite limitations [7, 8]. Thus, the resulting expansion of the colony surface makes the population grow linearly over time [8, 9], in contrast to the exponential growth in early colonies or liquid cultures. Therefore, the motility of cells is crucial to speed up colony expansion. It is well-established by swimming assays in low density hydrogel (~0.2% agar), that chemotaxis is enhanced by nutrient shortage [10–12] or attractant gradients [13]. Chemotaxis accelerates expansion dynamics of populations by allowing access to more nutrient [14]. In liquid media, the chemotaxis of the model bacterium *Escherichia coli* is driven by swimming, specifically

bundling and propelling of flagella, which gives rise to a run-and-tumble motion. In visco-elastic media, bacterial migration is restricted more and more as elasticity is raised and pore size diminished [15], and the chemotaxis has been reported to be reversely proportional to the elasticity of the medium [12]. Therefore, above a certain threshold of medium density, colony expansion is solely growth driven. Furthermore, in a dense hydrogel (>0.5% agarose), the stress at the interface (between colony and media) gives rise to internal ordering of cells [16]. But what happens in the intermediate regions, where the hydrogel is semi-dense? Is it possible that cells can both retain colony characteristics but still speed up the expansion to enhance colonization?

Here we use mono-clonal *E. coli* colonies embedded in an agarose matrix [2, 17] as simple models of 3D colony formation. We use a combination of experiments and mathematical modelling to show how 3D colonies can join growth and flagella-based motility to colonize their local environment. We investigate how the spreading depends on the expression of extra-cellular structures and hydrogel concentration. We demonstrate that indeed 3D colony expansion—driven by the combination of growth and motility—gives rise to satellite colony formation and acceleration of the population expansion to be super-linear over time.

## RESULTS

## Satellite colonies form around 3D colonies

To mimic 3D biofilm evolution in natural settings, *E. coli* MG1566 wild-type (wt) single cells were embedded in low concentration (~10 cells/ml) in a semi-dense agarose (0.3%) matrix and incubated for 15 h at 37°C in a minimal defined medium composed of M63 supplemented with 20 µM/ml glucose (M63 + glu). This protocol (Materials and Methods) resulted in confined,

<sup>1</sup>The Niels Bohr Institute, University of Copenhagen, Blegdamsvej 17, DK-2100 Copenhagen O, Denmark. ✉email: mitarai@nbi.dk; jauffred@nbi.dk

Received: 27 February 2023 Revised: 7 August 2023 Accepted: 8 August 2023  
Published online: 17 August 2023

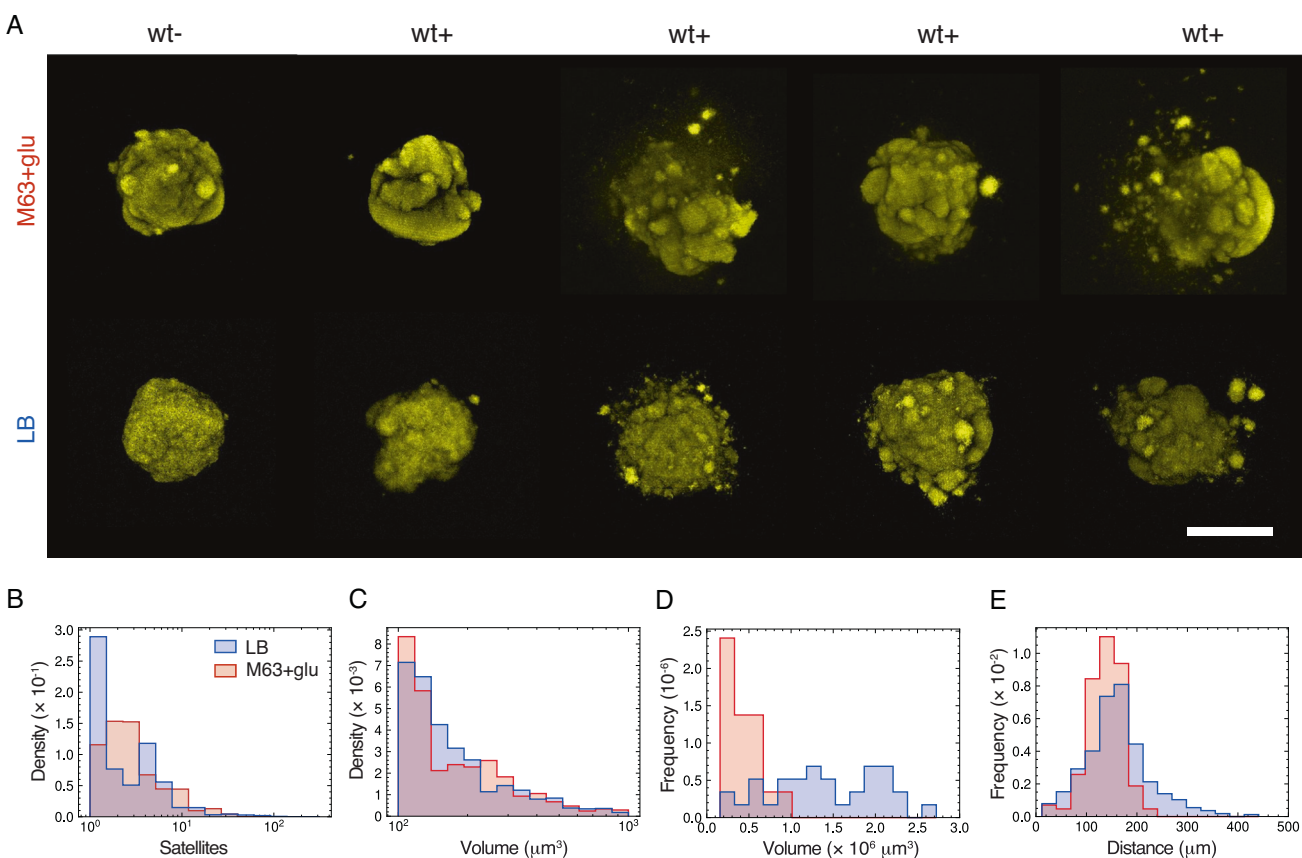


**Fig. 1 Satellite morphology in mature 3D colonies. A** Examples of pseudo-colored 3D colonies (maximum intensity projections) in 0.3% agarose and minimal (M63+glu) or rich medium (LB). These examples show inhomogeneity of morphologies without satellites (wt-) or with satellites (wt+). The scale bar corresponds to 200  $\mu\text{m}$ . **B** Distributions of the number of satellites pr. colony (log-scale) in either LB ( $N = 17$ ) and M63 + glu ( $N = 34$ ). **C** Distributions of satellite volumes (log-scale) in either LB ( $N = 149$ ) or in M63 + glu ( $N = 574$ ). **D** Distribution of volumes of the main colonies in either LB ( $N = 17$ ) and M63+glu ( $N = 34$ ). **E** Distributions of distances from the center-of-mass of satellites to the center-of-mass of the main colony in either LB ( $N = 17$ ) and M63 + glu ( $N = 34$ ).

mono-clonal quasi-spherical colonies on the order of a few hundred  $\mu\text{m}$  in diameter. We also verified that the colony expansion after 15 h has slowed down from exponential to become linear over time (Supplementary Fig. S1). In parallel, we performed a similar experiment using a rich Luria-Bertani (LB) medium and a shorter incubation time of 13 h to account for differences in doubling time in the two media: 27.8 min (LB) vs. 68.4 min (M63 + glu) (Supplementary Fig. S2). In similar studies, these has been referred to as 3D biofilms [16, 18, 19], but here we use the term colony.

The resulting colonies grew as compact quasi-spherical colonies with a mountainous surface of multiple protrusions, denoted as wt- (Fig. 1A, first column). However, for the majority of 3D colonies, 34/40 (M63 + glu) and 17/18 (LB), these protrusions seem to have escaped the colony as small stationary satellite colonies, denoted as wt+ (Fig. 1A). Both morphology types occurred for colonies grown in both the minimal (M63+glu) and the rich media (LB). It is worth noticing that these two morphologies were not determined by any obvious variations between experiments, as we found wt- and wt+ side by side in the same culture wells. To evaluate whether this behavior was dependent on the specific hydrogel, we did a similar assay interchanging agarose with agar (0.5%) and found the majority of 3D colonies, 21/39 (M63 + glu) to be wt+ (examples in Supplementary Fig. S3).

From the subset of 3D colonies with satellite morphology (wt+), we measured the distributions of number of satellites, their volumes, distances to the main colony, as well as the main colony volumes, for both minimal (blue) and rich (red) medium

(Fig. 1B-E). The distribution of the number of satellites per 3D colony (Fig. 1B) shows that the majority had less than 10 satellites. Furthermore, from the distribution of satellite volumes, we found that satellites with smaller volumes had higher prevalence (Fig. 1C). The typical satellite size ( $<10^3 \mu\text{m}^3$ ) was about three orders of magnitude smaller than the average volumes of the main colonies, which were  $(1.3 \pm 0.6) \cdot 10^6 \mu\text{m}^3$  (M63 + glu) and  $(4 \pm 1) \cdot 10^5 \mu\text{m}^3$  (LB) (Fig. 1D). Finally, the distributions of distances between center-of-masses of the satellites and their respective main colony had average distances of  $161 \pm 64 \mu\text{m}$  and  $137 \pm 35 \mu\text{m}$  for minimal (M63 + glu) and rich (LB) medium, respectively (Fig. 1E). Our definition of a satellite is that it is completely detached from the main colony. It is, therefore, possible that we wrongly exclude some of the smaller ( $<100 \mu\text{m}$ ) distances between the center-of-masses (Fig. 1E), as the satellites have partly merged with the main colonies. From time-lapse imaging we found incidences of satellites forming and subsequently merging with the main colony (Supplementary movies 1–5).

A possible mechanism behind satellite formation is the combination of bacterial cell-cell interaction, motility, and the growth of the cells: A few cells can move away from the surface of the main colony escaping from their attachment to migrate to a different position in the gel, and each of them starts to grow into a new satellite colony. Therefore, in the following, we investigate how bacterial surface structures, as well as the density of the substrate, affect the emergence of satellite colonies. The first is achieved by studying mutants with deletions of structures

important for adhesion and motility, and the latter by modifying agarose concentration in the extracellular matrix.

### Deletion of extracellular structures causes loss of satellite morphology

One of the factors governing the morphology of 3D colonies and the appearance of satellites must be the complex interplay between cell envelope components and the extracellular matrix. So, bacterial cell-adhesive structures, such as exo-polysaccharides (EPS), fimbriae, and flagella are obvious components that can modulate the colony morphology. Therefore, we investigated a collection of mutants lacking diverse bacterial surface structures (Table 1). Figure 2A sketches the parental strain (wt) and the suppressed structures: flagella, type I pili, colanic acid, curli fimbriae and antigen 43.

To examine the influence of these surface components, we examined the 3D colony morphology after knock-out deletion and compared it with the wt colony morphology (Fig. 2B).

Flagella are helical filaments responsible for some of the locomotion mechanisms adopted by bacteria. By expressing flagella, cells can self-propel in liquids (swimming) and on surfaces (swarming) [20]. Furthermore, flagella have been shown to play a role in cell–substratum (e.g. initial colony formation [21]) and cell–cell interactions [5]. However, the role of these structures in

bacterial motility in confined environments remains largely unknown [22]. We tested a  $\Delta fliC$  mutant and did not find any satellite formation ( $N=21$ ). We also assessed a  $\Delta fim$  mutant without type I pili, which is a hair-like structures crucial for cell–cell adhesion [21]. The morphology of these mutants was also indistinguishable from that of wt– ( $N=21$ ).

The  $\Delta flu$  mutant has a deletion in the gene encoding the auto-transporter protein antigen 43, which comes in high copy numbers (up to 50,000 pr. cell [23]). Antigen 43 favors cell–cell interactions through chain-formation and is referred to as a handshake protein [24–26]. Given the inverse regulation of pili and antigen 43 [27], we tested both  $\Delta flu$  ( $N=21$ ) and the double mutant  $\Delta flu\Delta fim$  ( $N=22$ ) and found that both display a loss of satellite morphology; even when agarose was interchanged with 0.5% agar (Supplementary Fig. S4).

We also tested the EPS colonic acid mutant,  $\Delta cps$  ( $N=17$ ), as well as the  $\Delta csgAB$  ( $N=18$ ) with a deletion in the gene encoding a fibrous surface protein, curli fimbriae, important for both cell–cell and cell–substrate adhesion [28–32]. Even though  $cps$  and  $csgAB$  predominantly are expressed at ambient temperature [30, 33], the wt has in a prior been found to have capsules in contrast to the EPS colonic acid mutant ( $\Delta cps$ ), which had none [34]. In accordance with that we found wt+ morphology to be lost in both cases. In summary, we found that the satellite morphology (wt+) is lost in the confined colonies of all tested mutants.

**Table 1.** *Escherichia coli* strains used in the study.

Name	Strain	Relevant characteristics	Reference
wt	MS613	MG1655 K-12 reference (F-lambda- ilvG- rfb-50 rph-1) strain	[62]
$\Delta flu$	MS427	MG1655 $\Delta flu$	[68]
$\Delta fim$	MS428	MG1655 $\Delta fim$	[24]
$\Delta flu\Delta fim$	MS528	MG1655 $\Delta flu\Delta fim$	[24]
$\Delta cps$	RMV340	MG1655cps::tet	[69]
$\Delta csgAB$	RMV612	MG1655csgAB::kan	[63]
$\Delta fliC$	NM109	MG1655fliC::kan	This study

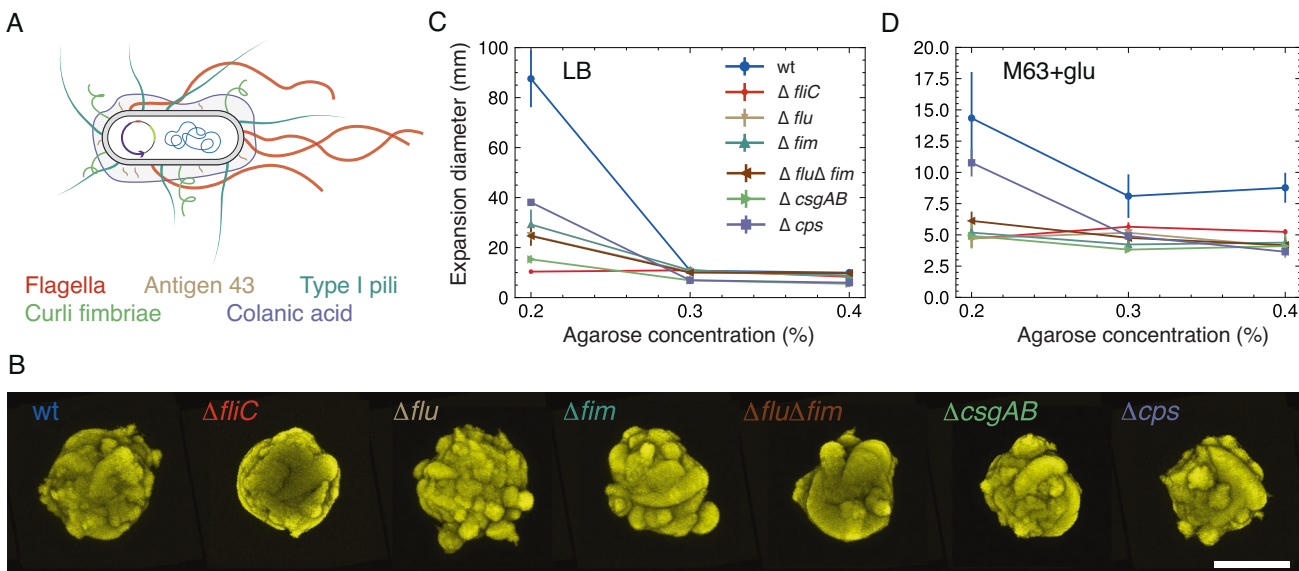


**Fig. 2** 3D morphology and motility of knock-out mutants. **A** Sketch of parental (wt) *E. coli* strain (not to scale). The sketched elements include the genome, the fluorescence-carrying plasmid and the extracellular structures: flagella (red), antigen 43 (beige), type I pili (dark green), curli fimbriae (light green), and colanic acid (purple). **B** Morphology of mutant 3D colonies. Examples of pseudo-colored fluorescent colonies (maximum intensity projections) grown in M63 + glu with 0.3% agarose. Scale bar corresponds to 200  $\mu$ m and color coding is the same as in (A). Swimming assay in low density agarose. Diameters of expansion zones after 24 h of incubation vs. agarose concentrations in LB (C) and M63 + glu (D).

non-flagellated mutant,  $\Delta fliC$ , but with large variations in speed. This is in accordance with the fact that many of the bacterial surface structures display interdependent regulation [35]. At higher substrate stiffness (0.3–0.4% agarose), where swimming is no longer the main driver of motility, the average moving distances were considerably reduced for all strains.

We also tested all strains' behavior in a minimal medium (M63 + glu) (Fig. 2D). In the low density minimal agarose (0.2%) the motility of all strains was reduced, as can be seen by comparing the maximum distance reached by wt: (14.3  $\pm$  3.7) cm vs. (87.5  $\pm$  11.4) cm in rich medium (LB). The reduced motility in minimal media is consistent with previous studies: it has been attributed to the considerable metabolic cost of producing flagella [36, 37], while a recent study [13] has shown that the chemotaxis is strongly reduced when there is no supplement attractant, even if the primary carbon source is also an attractant. Again, at greater agarose concentrations (0.3–0.4% agarose) motility was reduced to a non-detectable level for all other than the wt.

Overall, the low density agarose assay suggested that all the mutant strains tested here have reduced motility compared to the wt strain. This is in line with the view that the satellite colonies form as a compromise between their inherent motility and the mechanical constraints imposed by the environment.

#### Density of extra-cellular matrix controls satellite emergence

Another factor that affects both bacterial motility and colony morphology is the density of the enclosing matrix. To explore the colony morphology dependence on this environmental factor, we limited our analysis to a comparison between the highly motile wt and the non-flagellated mutant ( $\Delta fliC$ ) that was non-motile in all tested experimental settings. We investigated mono-clonal colonies of both strains in varying agarose concentration (0.25–0.35%) in rich (LB) and minimal (M63 + glu) medium.

As already mentioned, we found satellite morphology (wt+) among the 3D colonies in 0.3% agarose with frequencies of 34/40 and 17/18 for the wt strain in minimal and rich medium, respectively (Fig. 3). Namely, the satellite morphology was conserved despite changes in nutrient composition and possible slight changes in elasticity between the experimental samples [38].

When reducing the agarose concentration (0.25%) the distinct satellite morphology was lost for wt, and general spreading of the cells inside the gel was observed (Fig. 3, 0.25%). On the other hand, when stiffness was increased (0.35%), 3D colonies grew under greater confinement, resulting in the loss of wt+ morphology. In contrast, the non-motile strain ( $\Delta fliC$ ) always grew as single compact colonies at all tested agarose concentrations. We still observed the agarose concentration dependence on the morphology, as at 0.25% agarose concentration the surface of  $\Delta fliC$  colonies appeared more loosely connected than at higher agarose concentrations.

Colony surfaces became smoother as matrix stiffness increased for both strains (Fig. 3, 0.35%). In some cases

(7/18 in M63-glu and 6/9 in LB), we even found slightly oblate colony shapes. This shape change depends on the density of the environment, such that for higher stiffness (>0.4% agarose) all tested 3D colonies grew as single oblate colonies (Supplementary fig. S5), in agreement with earlier reports [39]. Recently, this shape morphology has been suggested to originate from the stiffness contrast between the colonies and the environment [16]. These findings all together suggest that the emergence of satellites is a transitional state between the morphologies: i) where cells can swim—more or less freely—through the extra-cellular matrix, and ii) where cells are strictly confined.

#### Satellite formation possibly speeds up colonization

The overall experimental result suggests that the observed satellite morphology is due to a combination of local growth of confined colonies and rare excursions of motile cells. Therefore,

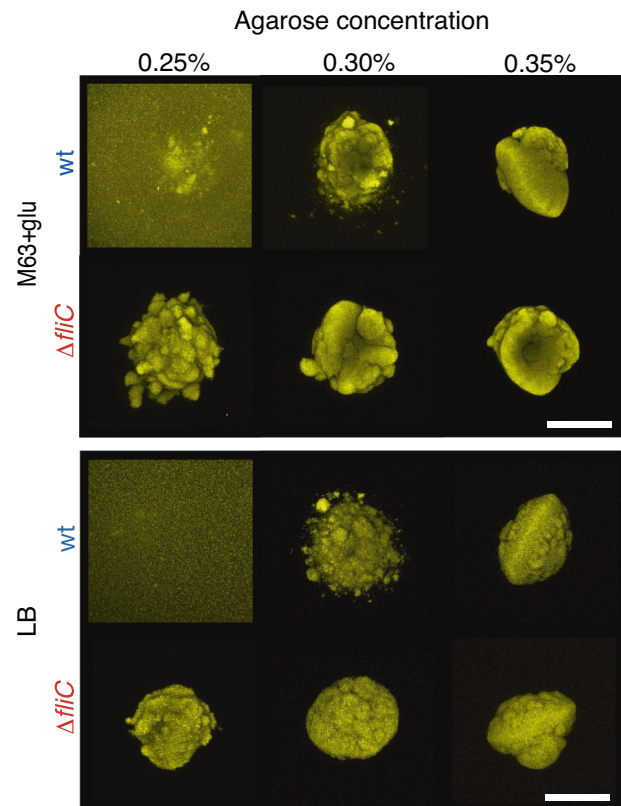


**Fig. 3 Effect on matrix density on 3D colony morphology.** Examples of pseudo-colored fluorescent parental (wt) or flagella mutant ( $\Delta fliC$ ) colonies (maximum intensity projections) grown in either minimal (M63+glu) or rich (LB) medium at various agarose concentrations. The scale bar corresponds to 200  $\mu$ m.

we propose a *simple* mathematical model of colony growth that has these two features and show that such a model indeed reproduces the 3D morphology of the confined bacterial colonies. We then used this model to further study how this mode of expansion can contribute to the overall colonization.

For this purpose, we modified the well-known Eden growth model, which is a lattice model, where the surface cells can divide to occupy empty nearest neighbor sites [40, 41]. Our modification allows for occasional escapes of single cells from the main colony. In other words, surface cells do not only grow but can also migrate to another empty site in the lattice. We assumed that the cells swim from site to site on timescales much faster than the time between two cell divisions (25–75 min, Supplementary Fig. S2). This assumption is based on the fact that cell divisions will decelerate swimming and experimental findings for *E. coli* in porous media [15]. So instead of simulating the cells' actual trajectory, we implemented the dispersal as a jump to a final position; chosen randomly by a radial Gaussian probability distribution centered around the starting site. Therefore, the model is essentially controlled by two parameters. The first is the rate of jumps,  $k_s$ , when the cell doubling rate,  $k$ , is set to unity. The second is the standard deviation,  $\sigma$ , of the Gaussian distribution of possible new sites to jump to. We ran the simulation until a million jump/division events. Thus, the resulting *in silico* colonies had widths of about 100  $\mu$ m assuming i) colonies are compact and ii) one occupied lattice site corresponds to one cell volume ( $\sim 1 \mu\text{m}^3$ ).

3D *in silico* colonies were obtained with  $\sigma \in \{2, 5, 7, 10\}$  and  $k_s \in \{0.001, 0.05, 0.1, 0.2\}$ . At low  $\sigma$  and  $k_s$ , the colonies were compact with smooth surfaces, as the distances ( $\sigma$ ) rise, small protrusions appear on the surface followed by satellite breakouts (Supplementary Fig. S6). As anticipated, the number of satellites also

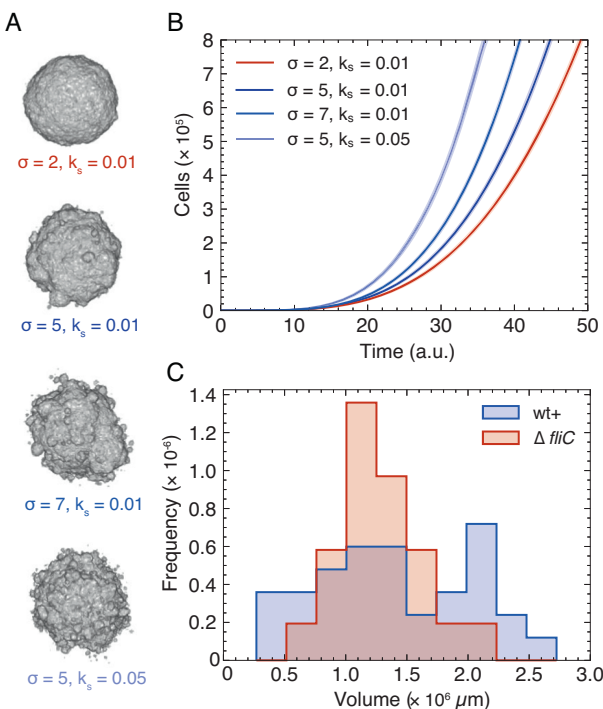


**Fig. 4 Population size and time evolution. A** Effect of frequency,  $k_s$ , and distance,  $\sigma$ , of jumps in the simulations of 3D colonies after  $10^6$  division/jump events; corresponding to motile (blue) and non-motile (red) colonies. **B** Time-evolution of each of the four examples ( $N = 25$ ) given in (A), where time is defined as detailed in Materials and methods. The shaded region corresponds to  $\pm\text{SD}$ . **C** Distribution of total colony volumes in minimal (M63+glu) medium of wt+ ( $N = 34$ ) and the flagella mutant  $\Delta\text{fl/C}$  ( $N = 21$ ). The wt+ corresponds to the sum of volumes in Fig. 1C+D (M63 + glu).

increased as the jump frequency ( $k_s$ ) increased and ultimately ( $\sigma = 10$  and  $k_s = 0.2$ ) the simulated system was no longer confined. Instead, the cells spread mimicking the experimental results of wt in the low density agarose assay (Fig. 3, 0.25%).

In this system, the smooth and compact colonies (Fig. 4A, red) mimic the non-motile  $\Delta\text{fl/C}$  colony (Fig. 2B) and the others (Fig. 4A, blue) different wt colonies (Fig. 1A). We analysed our in silico 3D colonies ( $N = 30$  of each) in the exact same way as in the experimental data (Fig. 1B-E) and found similar trends (Supplementary Fig. S7). With this we explored time evolution (Fig. 4B) and found that the colonies with wt+ morphology ( $\sigma = 5$  and  $k_s = 0.01$ ,  $\sigma = 7$  and  $k_s = 0.01$ , and  $\sigma = 7$  and  $k_s = 0.01$ ) clearly grew faster than the compact colonies ( $\sigma = 2$  and  $k_s = 0.01$ ). Hence, these results predict a view, where satellite outbreaks speed up the colonization of the extra-cellular matrix.

To test this prediction, we compared the experimental distributions of final total volumes of wt+ (blue) and  $\Delta\text{fl/C}$  (red) (Fig. 4C). We found that the occurrence of satellites results in a more widespread distribution of volumes compared to the non-motile strain ( $\Delta\text{fl/C}$ ). Surprisingly, there were also wt+ colonies with smaller volumes even though their doubling time may be slightly faster than that of  $\Delta\text{fl/C}$ : 68.4 min vs. 72.9 min (Supplementary Fig. S2). While the wide distribution makes it hard to compare the average values in the current sample size, the wider distribution with more satellite colonies is in qualitative accordance with the distributions of the simulated 3D colonies (Supplementary Fig. S8).

## DISCUSSION

Even though the flagella-mediated motility of *E. coli* is well-described by the run-and-tumble model [42], we still lack the full

understanding of how bacteria migrate through porous or visco-elastic media. Several theoretical works concerning flagella-based motility describe how the migration can be slowed down when colliding with structures of various sizes [43–45]. Moreover, in a recent study, the individual trajectories of bacteria in a porous medium were imaged and the velocity was found to be highly dependent on pore size [15]. Furthermore, agarose gels have “spongy” microstructures with a broad distribution of pore sizes. Particularly, for the semi-dense agarose (0.3%) used in this study, the pores range from a few hundred nanometers to a few micrometers (see ref. [46] Fig. 16 for a metastudy). Relating this to our results, the porous hydrogel will barely allow the bacteria to squeeze through. Altogether, these reports indicate that *E. coli* moves through a porous medium constantly alternating between stalling (being trapped), re-orientation, and swimming. In accordance with this, we find that flagella are necessary for migration through the various semi-dense media used in this study (Fig. 3). However, the behavior we observed is still very different from swimming in agarose (Fig. 2C+D) as the main colonies (as well as the satellites) in 0.3% agarose had sharply defined surfaces, indicating that cell outbreak is a rare event. Also, we did not see any signs of the collective colony detachments, recently reported in mature colonies [19, 47, 48].

Given these observations, we propose that the satellite colonies are formed by the rare—but not too rare—detachment and migration of a single surface cell, followed by stalling, and subsequent growth. So, the volumes of satellites indicate when, in the colony’s history, the excursion occurred. Furthermore, the size also tells us that the dispersal of the founder cell was long enough to allow the sub-cluster to form before it is annexed to the main colony. We observed that larger satellites ( $>500 \mu\text{m}^3$ ) were much less common (Fig. 3 wt LB 0.3% for an example) than smaller ones (Fig. 1B), which is consistent with the proposed mechanism.

Our lattice model, which is based on an Eden growth model with rare jumping events added, successfully produced 3D colonies with satellite morphologies in a specific parameter range. The model predicted that the distribution of total colony volumes would be more widespread when the satellite formation is more frequent (e.g. compare  $\sigma = 5$  and  $k_s = 0.05$  vs.  $\sigma = 2$  and  $k_s = 0.01$  in Supplementary Fig. S8). This is consistent with our experimental findings, where we find the distribution of total volumes of the flagella mutant ( $\Delta\text{fl/C}$ ) to be much narrower than for the parental (wt) strain (Fig. 4C).

Hallatschek and co-workers [49, 50] have theoretically demonstrated the impact of long-range dispersal in population expansion, especially when the dispersal distance distribution has a somewhat fat tail. In our model, the distribution of dispersion distances is Gaussian, but still the expansion dynamics of satellite-forming colonies is indeed faster than linear (Fig. 4B). On the other hand, it is also significantly slower than exponential growth (Supplementary Fig. S2). So, satellites form and then merge with the main colony and, thereby, limit the overall growth of the population. Nevertheless, our model suggests that in long term, the system will keep growing super-linearly, as the number of jumps (which is equivalent to the initialization of satellites) scales with the colony surface. In other words, as the growth of the main colony is linear (Supplementary Fig. S1) and the distribution of migration distances is unchanged over time, new satellites will keep forming and the main colony will never catch up with all the satellites. However, our model does not encompass spreading strategies on very long timescales, as the model ignores the effects of nutrient depletion and time-varying jumping distributions.

In our experiment, some of the main colonies of mutants produced very rough surfaces. Whilst the flagella knockout mutant’s surface ( $\Delta\text{fl/C}$ ) was overall smooth, the other mutants had several small protrusions of their surfaces (Fig. 2B). There are a few factors that can possibly contribute to the roughness of the

surfaces. The first is that even for the mutants, which are less motile than wt (Fig. 1C+D), individual surface cells escape occasionally. However, they travel significantly shorter distances than wt cells do. If this is the case, the satellites will quickly be re-absorbed into the main colony (Supplementary videos 1–5). In other words, the mountainous surface could be explained by motility with short dispersals (small  $\sigma$ ). This is also in accordance with the fact that higher agarose concentrations ( $>0.3\%$ ) resulted in smoother surfaces (Fig. 3). Another possibility is the nutrient driven instability of the surface growth. Several studies have shown how surface roughening instabilities are reinforced by the resulting local nutrient depletion [51]. The nutrient-driven instability also explains the (pseudo-fractal) broccoli-like morphology recently reported for 3D *E. coli* colonies [52]. It is possible that such instabilities are relevant, especially in the later stage of colony development. However, this effect is not included in our model since it does not consider space limitations and nutrient depletion separately.

Whilst the model compares well with our experimental results with respect to the distributions of satellites, main colony volumes, and distances to satellites (Fig. 1C–E vs. Supplementary Fig. S7B–D), it fails to reproduce the distributions of the number of satellites (Fig. 1B vs. Supplementary Fig. S7A). We conclude that with only two parameters ( $\sigma$  and  $k_s$ ), we cannot cover the varieties of the natural system or the rare successful escapes. We speculate that this could be related to the variance in flagella abundance, even among cells with the same genotype. It is well-known that the expression of flagella is highly heterogeneous, particularly that there are large stochastic variations in number of flagella. This has been suggested to be an evolutionary favorable strategy, as the expression of flagella is very energy consuming [53], such that motility is retained on colony level even when motility is limited on a cellular level.

Except for the mutant that did not express flagella, the studied strains lacked structures related to adhesion and aggregation processes rather than to motility. Still, we do not fully understand why the antigen 43 mutant ( $\Delta flu$ ) is less motile than the wt and—maybe as a result—hindered in satellite formation (Fig. 2). Biofilm formation has been shown to be associated with the expression of antigen 43 [24] and type I pili [21]. So one might assume that antigen 43 repression would up-regulate motility. However, the picture is more complex, as both EPS colonic acid [34] and type I pili [27] block antigen 43 function. Moreover, both antigen 43 and type I pili expressions are phase variable [54] and they are inversely regulated [55]. Therefore, more studies must be done to unravel the role of the surface structures *per se*, without the inverse regulations, phase variability, and physical shielding.

In general, dominant aggregation phenotypes are expected to hinder motility. Hence, it is reasonable to expect that when these processes are suppressed, the motility will increase. However, in our experiments, all the mutants presented reduced motility compared to their parental strain. This demonstrates the complexity of the bacterial motility phenotype. Indeed, vast amount of literature indicate the complex interdependence of motility and surface structure genes. Over-expression of the *handshake* protein antigen 43 (*flu*) has been reported to impair motility, not because of increased aggregation but due to interfering with the expression of flagella [56]. Similarly, the constitutive expression of type I fimbriae (*fim*) compromises the motility of bacteria by reducing the expression of flagellin [57]. The expression of curli (*csgAB*) and colanic acid (*cps*) are promoted by regulatory networks that down-regulate motility [58–60], therefore they are normally expressed in a complementary manner. Similar motility has been reported between wt and  $\Delta flu$  [56], and between strains with and without type I fimbrial expression [61], while this was not the case in our system (Fig. 2).

Taking our results together, we suggest that satellite-formation allows bacteria to colonize unknown horizons faster (super-linear

over time), whilst still retaining the tight bindings of the biofilm. Such spreading behavior can be advantageous, when invading complex environments, such as competing microbial communities, soils, or mammalian tissues. While we observed the phenomenon in a rather narrow range of the agarose concentrations, in nature it is likely that there are large gradients in the restriction of motility by the complexity of the matrix. If so, spreading through a semi-dense matrix using a combination of growth and occasional migrations, is a strategy, which ensures both fast invasion and stable occupation.

Whilst the flagella mutant's loss of satellites indicates the importance of flagella, more research is needed to explore how rare migratory events are enabled. For example, is it the inhomogeneity of gels that sometimes allows a cell to swim over long distances before being trapped? Or is it the cells that happen to express the relevant motility genes in high enough copy numbers to overcome the gel's resistance? Revealing the origin of the stochasticity behind rare excursions, may highlight unknown mechanisms of robust invasion of bacteria in complex environments.

## MATERIALS AND METHODS

### Bacterial strains and culture media

The *Escherichia coli* strains used in this study are derivatives of the wild-type MG1655 (K-12 F-lambda- ilvG- rfb-50 rph-1) [62] and are all listed in Table 1 and detailed in ref. [63] and references therein. However, the non-flagellated  $\Delta fliC$ , ( $\Delta fliC$ ::kan) mutant (NM109), was constructed specifically for this study through P1 transduction by moving  $\Delta fliC$ ::kan from JW1908-1 (Keio collection [64]) to MS613 followed by selection on kanamycin [65]. All strains were transformed with the plasmid pVS132 carrying an Isopropyl  $\beta$ -D-1-thiogalactopyranoside (IPTG) induced yellow fluorescent protein (YFP) and ampicillin resistance for selection [66] following a previously published protocol [67–69].

**Culture media.** Experiments were done using either of the two growth media: The rich Luria-Bertani (LB) composed of 1% tryptone, 0.5% NaCl and 0.5% yeast extract or M63 minimal media consisting of 20% 5  $\times$  M63 salt [70], 1  $\mu$ g/ml B1,  $2 \times 10^{-3}$  M MgSO<sub>4</sub>, and supplemented with 20  $\mu$ g/ml glucose (M63+glu). Both media were supplemented with 100  $\mu$ g/ml ampicillin, unless otherwise stated.

### Growth rate measurements

*E. coli* strains were grown overnight at 37 °C while shaking in either LB or M63+glu medium, before diluting 1000x in fresh medium without antibiotics. Initial OD<sub>600</sub> value (NanoPhotometer C40) was measured before incubation (37 °C) and repeated every hour.

### Swimming assay

Prior to experimentation, 96 mm dishes with 25 ml of either LB or M63+glu and various agarose concentrations: 0.2%, 0.3%, or 0.4% (w/v) were prepared and left to dry for 18 h on the bench. In parallel, strains were grown overnight while shaking (37 °C) in LB before inoculating 1  $\mu$ l in the middle of each dish. After 24 h of incubation (37 °C), the range diameters were measured.

### 3D bacterial colonies

*E. coli* strains were grown overnight at 37 °C while shaking in LB medium (OD<sub>600</sub>  $\approx$  4), before performing three consecutive thousand-fold dilutions until reaching a concentration of  $\approx 10^3$  cells/ml. Then cells were embedded in a transparent semi-dense matrix using the following procedure: First, media with 0.2–0.6% (w/v) agarose (SERVA cat. no. 11404) was melted (in a microwave) and shaken rigorously to ensure homogeneity. To minimize evaporation (and heat-induced aging [71]), we opened new 25 ml bottles of media and agarose each time, and made sure to avoid boiling. Secondly, media with agarose was aliquoted into 1 ml tubes and placed in a block-heater at 55 °C. After approximately 20 min, when the mixture had reached 55 °C, it was supplemented with ampicillin (100  $\mu$ g/ml) and 0.5 mM IPTG (for YFP induction). Then, 10  $\mu$ l of the diluted overnight culture was added and the mixture was immediately—to prevent untimely gelification and heat shocks—poured into a petri dish

(WillCo HBST-5040) with glass bottom. This results in a final concentration of  $\approx 10$  cells pr. well (i.e. 10 cells/ml). After a few minutes the mixture had solidified and the well was incubated upside-down ( $37^{\circ}\text{C}$ ) for 13 h (LB) or 15 h (M63 + glu) for all agarose concentrations: 0.2–0.6% (w/v). The different incubation times were chosen to balance different media-dependent growth rates (Supplementary Fig. S2). Using these small volumes, the matrix thickness was less than 400  $\mu\text{m}$ , which ensures a minimum of oxygen depletion. To check this further, we compared the number of satellites pr. Colony with the position in the well (z-direction) and found no obvious correlation. However, the cost of this thin layer is a high risk of the colonies growing onto (and spreading fast over) the surface. Therefore, we discarded all wells, with colonies where this kind of growth had happened.

To parallel this assay, agarose was interchanged with 0.5% (w/v) agar (BD Difco Bacto Dehydrated Agar, Fischer Scientific) following the exact same procedure as described above. However, we found that the resulting agar gel is softer than the agarose gel, so, the density of agar 0.5% matches ~0.3% agarose (Supplementary Fig. S9).

### Imaging of 3D bacterial colonies

3D colonies in microwell dishes were imaged with a laser-scanning confocal microscope (LSCM) (Leica, SP5) and a 20x air immersion objective (Nplan, L20x, 0.40corr  $\infty$ ). YFP was excited by an argon laser with a wavelength of 514 nm and emission was collected around  $550 \pm 30$  nm.

To estimate how the colony radius changes with time, colonies were imaged with an inverted Nikon Eclipse Ti fluorescent microscope (Nikon, Tokyo, Japan) using a 20x air immersion objective (Splan flour, L20x, 0.45- $\text{corr} \infty$ ) paired with an Andor Neo camera (Andor, Belfast, UK). YFP was excited by a Hg lamp and the emission was collected at  $535 \pm 30$  nm upon excitation at  $500 \pm 20$  nm with a frame rate of one every 40 min.

The same approach was taken for the time-lapse movies of growing colonies (Supplementary Movie 1–5), however, the frame rate was one every 50 min. The reason we used wide-field fluorescence instead of LSCM for time-lapses was to reduce bleaching and photo-toxicity.

**Morphology measurements.** For snapshots of 3D colonies, we collected z-stacks that captured the entire colony with (x,y)-resolution of 1.52  $\mu\text{m}$ /pixels and optimized z-resolution of 1.33  $\mu\text{m}$ . The total imaging time of the colony was on the order of few minutes.

### Image processing

As the typical penetration depth of a LSCM is around 100  $\mu\text{m}$  [72] and the dense colonies were of the order of 200  $\mu\text{m}$ , the part of the colony furthest away in the scanning-laser direction (z-direction) suffers from strong distortions. Therefore, the following analysis was restricted to the half-colony closest to the LSCM objective by cropping the collected fluorescence z-stack using a custom-made Fiji [73] routine. 3D image segmentation was done with BiofilmQ [74] using the Otsu method for thresholding. Lastly, background noise was removed by eliminating outlier voxels of clusters smaller than 11  $\mu\text{m}^3$ . The following BiofilmQ parameters were exported for subsequent analysis: Convexity, number of satellites, volumes, distances between center-of-masses, and nearest-neighbour objects. The same BiofilmQ parameters were exported for the *in silico* colonies, the thresholding step was skipped for them (as they are binary *per se*).

### Modified Eden growth model

To reproduce the features of the obtained experimental results a modified Eden growth model was implemented. In a three-dimensional cubic lattice of linear system size  $L$ , each lattice site can be occupied by at most one bacterial cell. Each cell can grow at a rate  $k$  if there is at least one empty site among their six next nearest-neighbour sites. On top of this, if three or more of the next nearest sites are empty, then in addition to the growth, the cell can jump to another location. This is implemented as a jump to a new randomly chosen location that happens at a rate  $k_s$ . This is implemented by counting the number of the cells that can only grow  $N_1$  and the number of cells that can both grow and swim  $N_2$  at each update and by applying a Gillespie algorithm. The initial condition is a single cell placed in the center of the system and then the following steps are iterated:

- Find all the cells in the lattice and count the number of their empty nearest-neighbours. Among them, a cell that has less than four

available neighbouring sites belongs to the population  $N_1$ , otherwise, the cell belongs to the population  $N_2$ .

- Define an array containing all empty neighbouring sites, corresponding to the surface of the colony.
- Compute the total event rate  $T = N_1 \cdot k + N_2 \cdot (k + k_s)$ , and determine the duration to the next event as  $\tau = -\ln(r)/T$ , where  $r$  is a random number from a uniform distribution ( $r = U \subseteq (0,1)$ ). Proceed the time by  $\tau$ .
- Draw a random uniform number,  $a$ , from a uniform distribution between zero and one ( $a = U \subseteq (0,1)$ ) and determine which event to happen by the following procedure:
  - If  $a > (N_1 + N_2) \cdot k/T$  a growing event happens. Choose a random surface site and add a new cell to it.
  - Otherwise, a swimming event happens. Choose a random cell of the sub-population  $N_2$ . Generate three random Gaussian distributed numbers of zero mean and standard deviation  $\sigma$ , to find the new position of the cell. If the new cell position is empty, update the cell position. If the new position is already occupied by another cell, draw a new position from the above-mentioned procedure until finding a new empty position.
- Return to (1).

Pseudo-code is provided in the Supplementary text.

### Statistics

All mean values are given as (mean  $\pm$  SD) unless stated otherwise and only when data are tested against the null hypothesis that it is normally distributed.

### DATA AVAILABILITY

The code to generate the simulated data is available in Zenodo with <https://doi.org/10.5281/zenodo.7414919>.

### REFERENCES

- Berlanga M, Guerrero R. Living together in biofilms: the microbial cell factory and its biotechnological implications. *Microb Cell Fact*. 2016;15:165.
- Eriksen RS, Svennengen SL, Sneppen K, Mitarai N. A growing microcolony can survive and support persistent propagation of virulent phages. *PNAS*. 2018;115:337–42.
- Hernández-Jiménez E, Del Campo R, Toledano V, Vallejo-Cremades MT, Muñoz A, Largo C, et al. Biofilm vs. planktonic bacterial mode of growth: which do human macrophages prefer? *BBRC*. 2013;441:947–52.
- Evans CR, Kempes CP, Price-Whelan A, Dietrich LE. Metabolic heterogeneity and cross-feeding in bacterial multicellular systems. *Trends Microbiol*. 2020;28:732–43.
- O'Toole G, Kaplan HB, Kolter R. Biofilm formation as microbial development. *Annu Rev Microbiol*. 2000;51:49–79.
- Tuson HH, Auer GK, Renner LD, Hasebe M, Tropini C, Salick M, et al. Measuring the stiffness of bacterial cells from growth rates in hydrogels of tunable elasticity. *Mol Microbiol*. 2012;84:874–91.
- Lavrentovich MO, Koschwanez JH, Nelson DR. Nutrient shielding in clusters of cells. *Phys Rev E*. 2013;87:062703.
- Lavrentovich MO, Nelson DR. Survival probabilities at spherical frontiers. *Theor Popul Biol*. 2015;102:26–39.
- Shao X, Mugler A, Kim J, Jeong HJ, Levin BR, Nemenman I. Growth of bacteria in 3-d colonies. *PLoS Comput Biol*. 2017;13:e1005679.
- Alon U, Surette MG, Barkai N, Leibler S. Robustness in bacterial chemotaxis. *Nature*. 1999;397:168–71.
- Sourjik V, Berg HC. Functional interactions between receptors in bacterial chemotaxis. *Nature*. 2004;428:437–41.
- Croze OA, Ferguson GP, Cates ME, Poon WC. Migration of chemotactic bacteria in soft agar: role of gel concentration. *Biophys J*. 2011;101:525–34.
- Cremer J, Honda T, Tang Y, Wong-Ng J, Vergassola M, Hwa T. Chemotaxis as a navigation strategy to boost range expansion. *Nature*. 2019;575:658–63.
- Lauffenburger D, Kennedy CR, Aris R. Traveling bands of chemotactic bacteria in the context of population growth. *Bull Math Biol*. 1984;46:19–40.
- Bhattacharjee T, Datta SS. Bacterial hopping and trapping in porous media. *Nat Commun*. 2019;10:2075.
- Zhang Q, Li J, Nijjer J, Lu H, Kothari M, Alert R, et al. Morphogenesis and cell ordering in confined bacterial biofilms. *PNAS*. 2021;118:e2107107118.

17. Burmølle M, Johnsen K, Al-Soud WA, Hansen LH, Sørensen SJ. The presence of embedded bacterial pure cultures in agar plates stimulate the culturability of soil bacteria. *J Microbiol Methods*. 2009;79:166–73.
18. Strathmann M, Griebe T, Flemming HC. Artificial biofilm model—a useful tool for biofilm research. *Appl Microbiol Biotechnol*. 2000;54:231–7.
19. Jung YG, Choi J, Kim SK, Lee JH, Kwon S. Embedded biofilm, a new biofilm model based on the embedded growth of bacteria. *Appl Environ Microbiol*. 2015;81:211–9.
20. Swiecicki JM, Sliusarenko O, Weibel DB. From swimming to swarming: *Escherichia coli* cell motility in two-dimensions. *Integr Biol*. 2013;5:1490–4.
21. Pratt LA, Kolter R. Genetic analysis of *Escherichia coli* biofilm formation: roles of flagella, motility, chemotaxis and type I pili. *Mol Microbiol*. 1998;30:285–93.
22. Du H, Xu W, Zhang Z, Han X. Bacterial behavior in confined spaces. *Front Cell Dev Biol*. 2021;9:629820.
23. Owen P, Caffrey P, Josefsson LG. Identification and partial characterization of a novel bipartite protein antigen associated with the outer membrane of *Escherichia coli*. *J Bacteriol*. 1987;169:3770–7.
24. Kjærgaard K, Schembri MA, Ramos C, Molin S, Klemm P. Antigen 43 facilitates formation of multispecies biofilms. *Environ Microbiol*. 2000;2:695–702.
25. Vejborg RM, Klemm P. Cellular chain formation in *Escherichia coli* biofilms. *Microbiology*. 2009;155:1407–17.
26. Diderichsen B, flu, a metastable gene controlling surface properties of *Escherichia coli*. *J Bacteriol*. 1980;141:858–67.
27. Hasman H, Chakraborty T, Klemm P. Antigen-43-mediated autoaggregation of *Escherichia coli* is blocked by fimbriation. *J Bacteriol*. 1999;181:4834–41.
28. Vidal O, Longin R, Prigent-Combaret C, Dorel C, Hooreman M, Lejeune P. Isolation of an *Escherichia coli* K-12 mutant strain able to form biofilms on inert surfaces: involvement of a new *ompR* allele that increases curli expression. *J Bacteriol*. 1998;180:2442–9.
29. Prigent-Combaret C, Vidal O, Dorel C, Lejeune P. Abiotic surface sensing and biofilm-dependent regulation of gene expression in *Escherichia coli*. *J Bacteriol*. 1999;181:5993–6002.
30. Prigent-Combaret C, Prensier G, Le Thi TT, Vidal O, Lejeune P, Dorel C. Developmental pathway for biofilm formation in curli-producing *Escherichia coli* strains: role of flagella, curli and colanic acid. *Environ Microbiol*. 2000;2:450–64.
31. Danese PN, Pratt LA, Dove SL, Kolter R. The outer membrane protein, antigen 43, mediates cell-to-cell interactions within *Escherichia coli* biofilms. *Mol Microbiol*. 2000;37:424–32.
32. Oh YJ, Hubauer-Brenner M, Gruber HJ, Cui Y, Traxler L, Siligan C, et al. Curli mediate bacterial adhesion to fibronectin via tensile multiple bonds. *Sci Rep*. 2016;6:33909.
33. Gualdi L, Tagliabue L, Bertagnoli S, Ierano T, De Castro C, Landini P. Cellulose modulates biofilm formation by counteracting curli-mediated colonization of solid surfaces in *Escherichia coli*. *Microbiology*. 2008;154:2017–24.
34. Schembri MA, Dalsgaard D, Klemm P. Capsule shields the function of short bacterial adhesins. *J Bacteriol*. 2004;186:1249–57.
35. Saldaña Z, Xicohtencatl-Cortes J, Avelino F, Phillips AD, Kaper JB, Puente JL, et al. Synergistic role of curli and cellulose in cell adhesion and biofilm formation of attaching and effacing *Escherichia coli* and identification of *fis* as a negative regulator of curli. *Environ Microbiol*. 2009;11:992–1006.
36. Bauchop T, Elsden SR. The growth of micro-organisms in relation to their energy supply. *Microbiology*. 1960;23:457–69.
37. Shehata TE, Marr AG. Effect of nutrient concentration on the growth of *Escherichia coli*. *J Bacteriol*. 1971;107:210–6.
38. Kandemir N, Vollmer W, Jakubovics NS, Chen J. Mechanical interactions between bacteria and hydrogels. *Sci Rep*. 2018;8:10893.
39. Mitchell AJ, Wimpenny JW. The effects of agar concentration on the growth and morphology of submerged colonies of motile and non-motile bacteria. *J Appl Microbiol*. 1997;83:76–84.
40. Neyman J. Proceedings of the fourth Berkeley symposium on mathematical statistics and probability. University of California Press; Berkeley, California; 1961.
41. Jullien R, Botet R. Surface thickness in the Eden model. *Phys Rev Lett*. 1985;54:2055.
42. Jarrell KF, McBride MJ. The surprisingly diverse ways that prokaryotes move. *Nat Rev Microbiol*. 2008;6:466–76.
43. Duffy KJ, Cummings PT, Ford RM. Random walk calculations for bacterial migration in porous media. *Biophys J*. 1995;68:800–6.
44. Frangipane G, Vizsnyiczai G, Maggi C, Savo R, Sciotino A, Gigan S, et al. Invariance properties of bacterial random walks in complex structures. *Nat Commun*. 2019;10:2442.
45. Licata NA, Mohari B, Fuqua C, Setayeshgar S. Diffusion of bacterial cells in porous media. *Biophys J*. 2016;110:247–57.
46. Ed-Daoui A, Snabre P. Poroviscoelasticity and compression-softening of agarose hydrogels. *Rheol Acta*. 2021;60:327–51.
47. Petrova OE, Sauer K. Escaping the biofilm in more than one way: desorption, detachment or dispersion. *Curr Opin Microbiol*. 2016;30:67–78.
48. Sauer K, Stoodley P, Goeres DM, Hall-Stoodley L, Burmølle M, Stewart PS, et al. The biofilm life cycle: expanding the conceptual model of biofilm formation. *Nat Rev Microbiol*. 2022;20:608–20.
49. Hallatschek O, Fisher DS. Acceleration of evolutionary spread by long-range dispersal. *PNAS*. 2014;111:4911–9.
50. Paulose J, Hallatschek O. The impact of long-range dispersal on gene surfing. *PNAS*. 2020;117:7584–93.
51. Matsushita M, Wakita J, Itoh H, Ràfols I, Matsuyama T, Sakaguchi H, et al. Interface growth and pattern formation in bacterial colonies. *Phys A Stat Mech*. 1998;249:517–24.
52. Martínez-Calvo A, Bhattacharjee T, Bay RK, Luu HN, Hancock AM, Wingreen NS, et al. Morphological instability and roughening of growing 3D bacterial colonies. *PNAS*. 2022;119:2208019119.
53. Klumpp S, Zhang Z, Hwa T. Growth rate-dependent global effects on gene expression in bacteria. *Cell*. 2009;139:1366–75.
54. Hasman H, Schembri MA, Klemm P. Antigen 43 and type 1 fimbriae determine colony morphology of *Escherichia coli* K-12. *J Bacteriol*. 2000;182:1089–95.
55. Schembri M, Ussery D, Workman C, Hasman H, Klemm P. DNA microarray analysis of *fim* mutations in *Escherichia coli*. *Mol Genet Genom*. 2002;267:721–9.
56. Ulett GC, Webb RL, Schembri MA. Antigen-43-mediated autoaggregation impairs motility in *Escherichia coli*. *Microbiology*. 2006;152:2101–10.
57. Simms AN, Mobley HL. Multiple genes repress motility in uropathogenic *Escherichia coli* constitutively expressing type 1 fimbriae. *J Bacteriol*. 2008;190:3747–56.
58. Sommerfeldt N, Possling A, Becker G, Pesavento C, Tschowri N, Hengge R. Gene expression patterns and differential input into curli fimbriae regulation of all GGDEF/EAL domain proteins in *Escherichia coli*. *Microbiology*. 2009;155:1318–31.
59. Wang Q, Zhao Y, McClelland M, Harshey RM. The RcsCDB signaling system and swarming motility in *Salmonella enterica* serovar Typhimurium: dual regulation of flagellar and SPI-2 virulence genes. *J Bacteriol*. 2007;189:8447–57.
60. Pesavento C, Becker G, Sommerfeldt N, Possling A, Tschowri N, Mehlis A, et al. Inverse regulatory coordination of motility and curli-mediated adhesion in *Escherichia coli*. *Genes Dev*. 2008;22:2434–46.
61. Lane MC, Simms AN, Mobley HL. Complex interplay between type 1 fimbrial expression and flagellum-mediated motility of uropathogenic *Escherichia coli*. *J Bacteriol*. 2007;189:5523–33.
62. Bachmann B. *Escherichia coli* and *Salmonella*: Cellular and molecular biology. p 2460–2488; Editor: Neidhardt F.C. ASM Press; Washington DC 1996.
63. Jauffred L, Munk Vejborg R, Korolev KS, Brown S, Oddershede LB. Chirality in microbial biofilms is mediated by close interactions between the cell surface and the substratum. *ISME J*. 2017;11:1688–701.
64. Baba T, Ara T, Hasegawa M, Takai Y, Okumura Y, Baba M, et al. Construction of *Escherichia coli* K-12 in-frame, single-gene knockout mutants: the Keio collection. *Mol Syst Biol*. 2006;2:2006.
65. Silhavy TJ, Berman ML, Enquist LW. Experiments with gene fusions. Cold Spring Harbor Laboratory; Cold Spring Harbor, New York; 1984.
66. Hallatschek O, Hersen P, Ramanathan S, Nelson DR. Genetic drift at expanding frontiers promotes gene segregation. *PNAS*. 2007;104:19926–30.
67. Cohen SN, Chang AC, Hsu L. Nonchromosomal antibiotic resistance in bacteria: genetic transformation of *Escherichia coli* by R-factor DNA. *PNAS*. 1972;69:2110–4.
68. Reisner A, Haagensen JA, Schembri MA, Zechner EL, Molin S. Development and maturation of *Escherichia coli* K-12 biofilms. *Mol Microbiol*. 2003;48:933–46.
69. Beloin C, Michaelis K, Lindner K, Landini P, Hacker J, Ghigo JM, et al. The transcriptional antiterminator RfaH represses biofilm formation in *Escherichia coli*. *J Bacteriol*. 2006;188:1316–31.
70. Elbing K, Brent R. Media preparation and bacteriological tools. *Curr Protoc Mol Biol*. 2002;59:1.1.1–1.1.7.
71. Mao B, Bentaleb A, Louerat F, Divoux T, Snabre P. Heat-induced aging of agar solutions: Impact on the structural and mechanical properties of agar gels. *Food Hydrocoll*. 2017;64:59–69.
72. Graf BW, Boppert SA. Imaging and analysis of three-dimensional cell culture models. *Methods Mol Biol*. 2010;591:211–27.
73. Schindelin J, Arganda-Carreras I, Frise E, Kaynig V, Longair M, Pietzsch T, et al. Fiji: an open-source platform for biological-image analysis. *Nat Methods*. 2012;9:676–82.
74. Hartmann R, Jeckel H, Jelli E, Singh PK, Vaidya S, Bayer M, et al. Quantitative image analysis of microbial communities with biofilmQ. *Nat Microbiol*. 2021;6:151–6.

## AUTHOR CONTRIBUTIONS

All authors developed the theory and MC performed the experiments and the computations. LJ and NM verified the analytical methods and supervised the findings of this work. All authors discussed the results and contributed to the final manuscript.

**FUNDING**

Open access funding provided by Royal Library, Copenhagen University Library.

**COMPETING INTERESTS**

The authors declare no competing interests.

**ADDITIONAL INFORMATION**

**Supplementary information** The online version contains supplementary material available at <https://doi.org/10.1038/s41396-023-01494-x>.

**Correspondence** and requests for materials should be addressed to Namiko Mitarai or Liselotte Jauffred.

**Reprints and permission information** is available at <http://www.nature.com/reprints>

**Publisher's note** Springer Nature remains neutral with regard to jurisdictional claims in published maps and institutional affiliations.



**Open Access** This article is licensed under a Creative Commons Attribution 4.0 International License, which permits use, sharing, adaptation, distribution and reproduction in any medium or format, as long as you give appropriate credit to the original author(s) and the source, provide a link to the Creative Commons licence, and indicate if changes were made. The images or other third party material in this article are included in the article's Creative Commons licence, unless indicated otherwise in a credit line to the material. If material is not included in the article's Creative Commons licence and your intended use is not permitted by statutory regulation or exceeds the permitted use, you will need to obtain permission directly from the copyright holder. To view a copy of this licence, visit <http://creativecommons.org/licenses/by/4.0/>.

© The Author(s) 2023